View Journal

click for updates

PCCP

Accepted Manuscript

Volume 18 | Number 1 | 7 January 2016 | Pages 1–636

PCCP

Physical Chemistry Chemical Physics
www.rsc.org/pccp

ISSN 1463-9076

ROYAL SOCIETY OF CHEMISTRY

PERSPECTIVE
Darya Radziuk and Helmuth Möhwald
Ultrasonically treated liquid interfaces for progress in cleaning and separation processes

175 YEARS

This is an Accepted Manuscript, which has been through the Royal Society of Chemistry peer review process and has been accepted for publication.

Accepted Manuscripts are published online shortly after acceptance, before technical editing, formatting and proof reading. Using this free service, authors can make their results available to the community, in citable form, before we publish the edited article. We will replace this Accepted Manuscript with the edited and formatted Advance Article as soon as it is available.

You can find more information about Accepted Manuscripts in the **author guidelines**.

ROYAL SOCIETY OF CHEMISTRY

rsc.li/pccp

Molecular aggregation of naphthalimide organic semiconductors assisted by amphiphilic and lipophilic interactions: a joint theoretical and experimental study

I. Arrechea-Marcos,[a] P. de Echegaray,[b,c] M.J. Mancheño,[b] M. C. Ruiz Delgado,[a] M. M. Ramos,[c] J. A. Quintana,[d] J. M. Villalvilla,[e] M. A. Díaz-García,[e] J. T. López Navarrete,[a*] R. Ponce Ortiz,[a*] J.L. Segura[b*]

[a]*Departmento de Química Física, Universidad de Málaga, Málaga, 29071, Spain.*
[b]*Departmento de Química Orgánica I, Facultad de Química, Universidad Complutense de Madrid, Madrid, E-28040 Madrid, Spain.*
[c]*Departamento de Tecnología Química y Ambiental, Universidad Rey Juan Carlos, Madrid 28933, Spain*
[d] *Dpto. Óptica, Instituto Universitario de Materiales de Alicante y Unidad Asociada UA-CSIC, Universidad de Alicante, 03080 Alicante, Spain.*
[e] *Dpto. Física Aplicada, Instituto Universitario de Materiales de Alicante y Unidad Asociada UA-CSIC, Universidad de Alicante, 03080 Alicante, Spain.*

E-mail: teodomiro@uma.es; rocioponce@uma.es; segura@quim.ucm.es

Abstract

Amphiphilic and lipophilic donor-acceptor naphthalimide-oligothiophene assemblies exhibiting almost identical intramolecular properties, but differing in their intermolecular interactions, have been synthesized. Here we analyze the effect of replacing the normally used lipophilic alkyl chains by hydrophilic ones in directing molecular aggregation from an antiparallel to a parallel stacking. This different molecular packing of the amphiphilic, **NIP-3T**$_{\textbf{Amphi}}$, and lipophilic, **NIP-3T**$_{\textbf{Lipo}}$, systems is assessed by electronic spectroscopies, scanning electronic microscopy and DFT quantum-chemical calculations. Theoretical calculations indicate that the presence of amphiphilic interactions promotes a face-to-face parallel arrangement of neighbor molecules which induces improved electronic coupling and therefore, enhances the charge transport ability and photoconducting properties of this type of materials. Time of flight and photoconducting measurements are used to determine the impact of the amphiphilic and lipophilic interactions on their possible performance in optoelectronic devices.

Introduction

Donor (D)–acceptor (A) oligothiophene derivatives have received a great deal of attention due to their interesting electrochemical properties which make them interesting candidates for ambipolar field-effect charge transport as well as because of their varied photophysical properties.[1-3] Especially remarkable has been the investigation on different oligothiophenes covalently linked to naphthalimides,[4-6] the smallest member of the rylene colorant family,[7, 8] because of their significance as organic materials and in supramolecular chemistry.[9] Thus, in the last few years we have synthesized
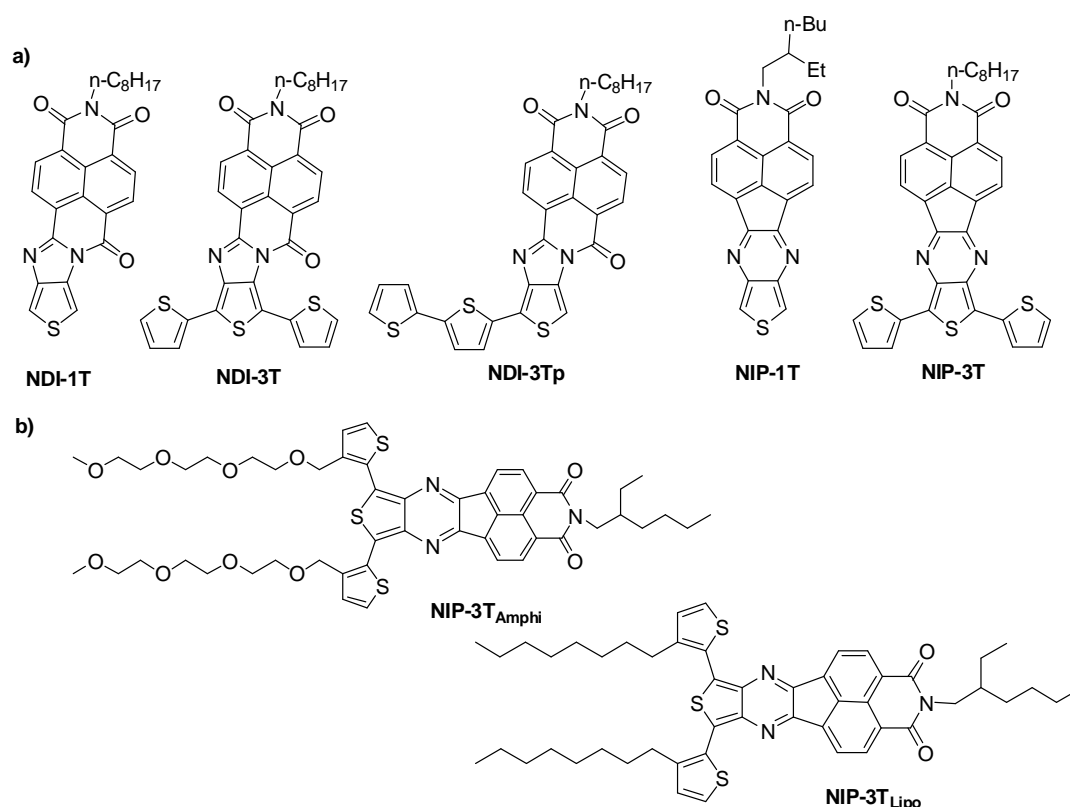

Figure 1. (a) Molecular structure of oligothiophene-naphthalimide assemblies synthesized in our group with good performances in OFETs and (b) new oligothiophene-naphthalimide assemblies investigated in this article.

oligothiophene-naphthalimide and peryleneimide assemblies (Figure 1a) with good performances in organic field-effect transistors (OFETs)[10, 11] in which both donor and acceptor moieties are directly conjugated through either imidazole or pyrazine rigid linkers. It was found that the absence of skeletal distortions allows closer intermolecular π-π stacking and enhances intramolecular π-conjugation, thus promoting good film crystallinity and low reorganization energies for both electron and hole transport.[11, 12]

In this context, tailoring electron donor (D)–acceptor (A) heterojunctions is one of the most essential subjects in the design of optoelectronic materials. D and A components tend to assemble together via a charge-transfer (CT) interaction,[13-15] unfavorable for photoelectric conversion and charge transport. Thus, X-Ray diffraction of single crystal of some of our previously synthesized derivatives of these families (Figure 1) show that the conjugated D-A molecules stack with neighboring molecules packing in a head-to-tail fashion. This should not be in principle a problem for photoelectric conversion and charge transport, [10] if the frontier molecular orbitals were delocalized over the whole conjugated skeleton.[16] However, in systems closely related with these semiconductors,[10, 12] we have demonstrated that the HOMO and LUMO levels are localized on the oligothiophene and arylene fragments, respectively.

Therefore, rational molecular assembling strategies are needed to assist donor (D) and acceptor (A) molecules to assemble homotropically to form heterojunctions with segregated D and A domains for transporting holes and electrons, respectively.[17-23] This essential problem has been already addressed by Aida and coworkers, who proposed a molecular design strategy using 'side-chain incompatibility' based on D-A dyads site-specifically functionalized with two incompatible side chains.[24,25] Other interesting examples also proposing the use of amphiphilic chains to form active gels can be found in literature.[26-32]

On the basis of our previous work, we have adapted this molecular design to the development of new molecular semiconductors named **NIP-3T$_{Amphi}$** and **NIP-3T$_{Lipo}$** (Figure 1b), which bear at their termini hydrophilic and hydrophobic side chains, respectively. Our final aim is to relate the optoelectronic properties of the materials with the different self-assembling behavior of the amphiphilic and lipophilic systems. Note that tuning the molecular packing in organic semiconductors normally has tremendous influence on the electronic properties.[29-31]

Our molecular design consists of naphthalimide-fused thienopyrazine (NIP) derivatives **NIP-3T$_{Amphi}$** and **NIP-3T$_{Lipo}$** with A-D units. The donor moiety consists of terthiophene units connected by a pyrazine linker to the naphthalimide. The **NIP-3T$_{Lipo}$** possesses a hydrophobic structure with alkyl chains in both sides of the NIP core while the **NIP-3T$_{Amphi}$** derivative is designed with an unsymmetrical amphiphilic structure provided by *N*-alkylimide functionality and triethylene glycol (TEG) chains on the opposite sides, which may allow self-assembly by noncovalent interactions, whereas hydrophobic–hydrophilic interactions may play a determinant role for aggregation [33-

[36,37]. Thus, we expect that the novel amphiphilic structures might subsequently stack themselves to form highly ordered aggregates compared to non-amphiphilic **NIP-3T$_{Lipo}$**.

Results and discussion

Synthesis

As mentioned above, **NIP-3T$_{Lipo}$** possesses hydrophobic alkyl chains on both sides of the molecule while **NIP-3T$_{Amphi}$** exhibits a hydrophobic alkyl chain on one side of the NIP core and a hydrophilic tetraethyleneglycole (TEG) chain on the other one. To

Scheme 1

Physical Chemistry Chemical Physics Accepted Manuscript
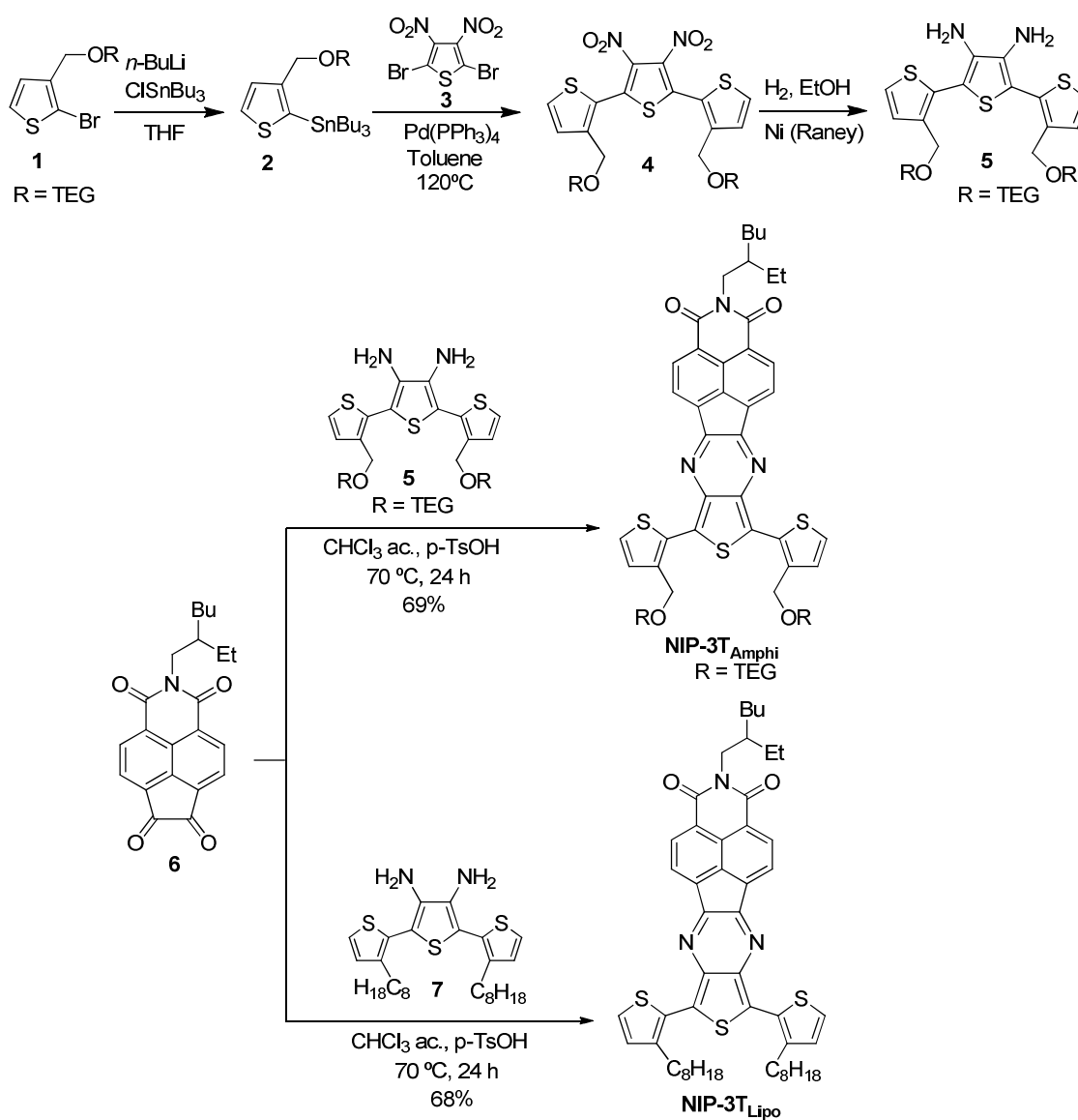
achieve the asymmetric functionalization of the NIP core, a convergent strategy with stepwise introduction of hydrophobic or hydrophilic terthiophene segments to the naphtalimide dione building block **6** was adopted (Scheme 1).

Diamine **5** was obtained by the three-step reaction sequence depicted in Scheme 1 starting from a 2-bromothiophene derivative endowed with a TEG chain (**1**). Stannilation reaction of **1** provided thiophene derivative **2** which was further reacted via Stille cross-coupling reaction with 2,5-dibromo-3,4-dinitrothiophene (**3**) to afford the dinitroterthiophene derivative **4**. Further reduction of **4** with H_2/Ni(Ra) in ethanol solution provided the target diaminoterthiophene derivative **5** endowed with a hydrophilic TEG chain. Condensation reactions between the versatile diketone **6**[38] and diaminoterthiophene derivatives **5** and **7**[39]in acid catalyzed chloroform solution, yielded respectively **NIP-3T$_{Amphi}$** and **NIP-3T$_{Lipo}$** as blue solids in 69 and 68 % yields (Scheme 1).

Both oligothiophene-naphthalimide assemblies possess excellent solubility in common organic solvents. Thus, **NIP-3T$_{Amphi}$** was highly soluble in THF, CH_2Cl_2, $CHCl_3$, MeOH, MeCN, acetone and dioxane at room temperature. This can be attributed to both the polyoxyethylene and *n*-alkyl side-chains. **NIP-3T$_{Lipo}$** was also soluble in the same solvents with the exception of MeOH.

The novel oligothiophene-naphthalimide assemblies were characterized by NMR, optical spectroscopies as well as HRMS (see Synthetic details in SI). As expected, ^{1}H NMR spectra of all derivatives are quite alike for the protons located in the aliphatic region assigned to the *N*-alkyl chain, thus the first CH_2 groups attached to nitrogen atoms of the imide cores appear around 4.14 ppm. A broad signal can be assigned for the C*H* group around 1.94 ppm and the rests of the protons assignable to the branched alkyl or TEG chains are in the usual range.

The same similarities are observed for aromatic and aliphatic carbons in ^{13}C NMR for both derivatives. Thus, imide groups appear around 164 ppm and all thiophene carbons are located in the normal range. Branched alkyl chains show the N-CH_2 around 44.5 ppm and C*H* appears at 38.3 ppm. Otherwise, TEG chains appear downfield in the range of 68-72 ppm for OCH_2 and 59.1ppm for the OCH_3 groups. Finally, FTIR spectra of both compounds clearly evidence the presence of the imide groups at 1705 and 1669 cm^{-1} (see Synthetic details in SI).

Stability of the samples was established by thermal gravimetric analysis (TGA), both exhibiting moderate thermal stability, with losses higher than 5% at temperature of 123

ºC and 191 ºC for **NIP-3T$_{Amphi}$** and **NIP-3T$_{Lipo}$**, respectively (see SI, Figures S1 and S2).

Electrochemical and optical characterization

In order to determine that any changes in the optoelectronic properties of the two semiconductors are related to a different packing structure, one must rule out that the substitution with different alkyl/alkoxy chains have any remarkable impact of the semiconductors electronic and optical properties. With this in mind, we have performed cyclic voltammetry measurements (Figure 2, Table 1) in dichloromethane solutions using tetrabutylammoniumhexafluorophosphate (TBAHFP) 0.1 M as the supporting electrolyte and platinum as the working and counterelectrodes. As reference electrode we use Ag/AgCl and the potentials were referenced against the Ferrocene/ferrocenium redox couple (0.52 V *vs*. SCE). These measurements allow us to calculate the HOMO and LUMO levels precisely.
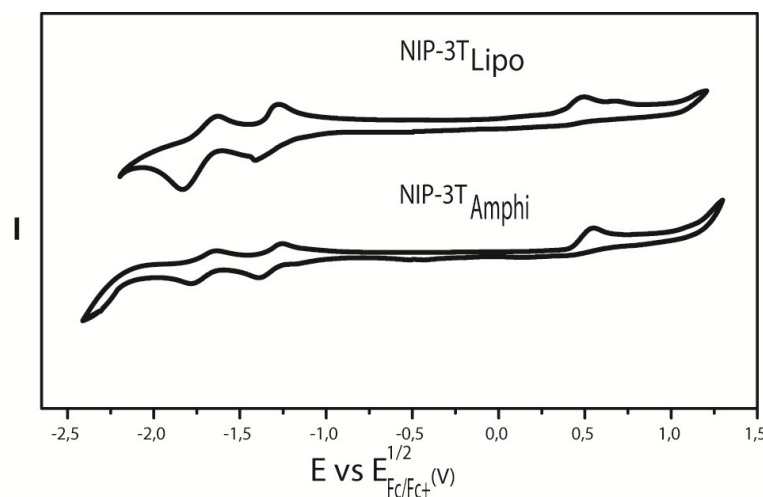

Figure 2. Cyclic voltammograms of **NIP-3T$_{Lipo}$** (top) and **NIP-3T$_{Amphi}$** (bottom) in dichloromethane solutions.

As expected, the different alkyl/alkoxy chains do not have a remarkable effect in the electrochemical properties. In fact, both compounds exhibit an almost identical electrochemical response. They show two reversible reduction processes which can be assigned to the naphthalimide moiety while the oligothiophene moiety is responsible for

the oxidation processes. We have also estimated the ionization potential (E_{HOMO}) and electron affinity (E_{LUMO}) values for the novel semiconductors from the oxidation and reduction potential data by using standard approximations[10,40-42] and they show almost identical values (Table 1).

The same occurs in the optical characterization. Thus, the absorption spectra of **NIP-3T$_{Lipo}$** and **NIP-3T$_{Amphi}$** recorded in dichloromethane solutions (Figure 3a) are nearly identical, showing two characteristic bands with maximums at 346 and 520 nm for **NIP-3T$_{Lipo}$** and at 345 and 526 nm for **NIP-3T$_{Amphi}$**, again indicating that the substitution of an alkyl chain by an alkoxy one have a negligible effect on the intramolecular electronic properties. Note also that, due the presence of both polar and apolar chains, **NIP-3T$_{Amphi}$** is soluble both in apolar and polar solvents, and its absorption spectra show basically no changes with polarity (see Figure 3b). The broad absorption band centered at *ca* 520 nm for both compounds can be assigned to an intramolecular charge-transfer (ICT) excitation. The intramolecular charge-transfer nature of this band has been previously theoretically confirmed by TDDFT calculations carried out on the parent **NIP-3T**[12] (Figure 1a) and indicates the spatial separation of the HOMO and LUMO orbitals stated above. Therefore, this transition can be described as a one-electron HOMO–LUMO excitation, consisting of displacement of the electron density from the HOMO, primarily localized on the oligothiophene fragment, to the LUMO, localized on the naphthalimide unit (see molecular orbital topologies in Figure S3). The optical bandgaps estimated from the onset of the lowest energy absorptions are quite similar to the electrochemical bandgaps (Table 1). Thus, we can conclude that the absorption spectral profiles and redox properties of **NIP-3T$_{Amphi}$** and **NIP-3T$_{Lipo}$** are nearly identical under these diluted conditions.

Table 1. UV/Vis absorption onsets (λ_{ons}), maxima (λ_{max}), optical band gap (E_{GAP}^{OPT}), reduction (E_{red}) and oxidation (E_{ox}) potentials, E_{HOMO} and E_{LUMO}.

Compound	λ_{max} nm	λ_{ons} nm	E_{GAP}^{OPT} eV	$E_{red(I)}^{1/2}$ V	$E_{red(II)}^{1/2}$ V	$E_{ox(I)}$ V[d]	$E_{ox(II)}$ V[d]	E_{LUMO} V	E_{HOMO} V	E_{GAP}^{ELEC} eV
NIP-3T$_{Amphi}$	346, 520	639	1.94	-1.32	-1.70	0.55	-	-3.78	-5.65	1.87
NIP-3T$_{Lipo}$	345, 526	659	1.88	-1.33	-1.72	0.49	0.68	-3.77	-5.59	1.82

[a] Referenced to the Fc/Fc$^+$ couple in CH$_2$Cl$_2$ (0.52 V *vs*. SCE). [b] LUMO level estimated from E_{LUMO}=-(E_{red}+5.1) (eV); HOMO level estimated from E_{HOMO}=-(E_{ox}+5.1) (eV). [c] E_{GAP}^{ELEC} = E_{LUMO} - E_{HOMO}. [d] Anodic potentials.

The UV-Vis absorption spectra of the novel assemblies in solid state have been recorded using drop-cast films from 1.9×10^{-7} M and 2.9×10^{-7} M solutions in CH_2Cl_2 of **NIP-3T$_{Amphi}$** and **NIP-3T$_{Lipo}$**, respectively (Figure 3c and 3d). The films were deposited over a quartz surface. For both compounds it is observed a considerable bathochromic shift in comparison with the UV-Vis absorption spectra in solution, suggestive of considerable aggregation of both assemblies in the condensed state.

In order to get some insight in the aggregation processes, we have carried out concentration dependent electronic absorption spectra (1.95×10^{-5} M to 7.8×10^{-7} M) of **NIP-3T$_{Amphi}$** in pure methanol, DCM or *n*-hexane (Figure S4). In this range of concentrations, no obvious shift was observed in the absorption spectra. Similar studies of **NIP-3T$_{Lipo}$** were carried out, showing no shifts when varying the concentration (see Figure S5). However, some differences are observed when the absorption spectra of both derivatives, **NIP-3T$_{Amphi}$** and **NIP-3T$_{Lipo}$,** are recorded in different mixtures of THF/H_2O, therefore increasing the medium polarity (Figures S6 and S7). While the absorption spectra of **NIP-3T$_{Amphi}$** do not change in THF/H_2O solvent mixtures with proportions varying from 100/0 to 40/60, in the case of **NIP-3T$_{Lipo}$**, for solvents mixtures more polar than 60/40 (THF/H_2O), the low energy band redshifts, resembling the thin film absorption spectra. These results indicate the formation of **NIP-3T$_{Lipo}$** aggregates under such conditions, due to decreased solubility. Note however that a further polarity increase, up to THF/H_2O mixtures (10:90), provokes the formation of aggregates in both molecules (Figure S7).
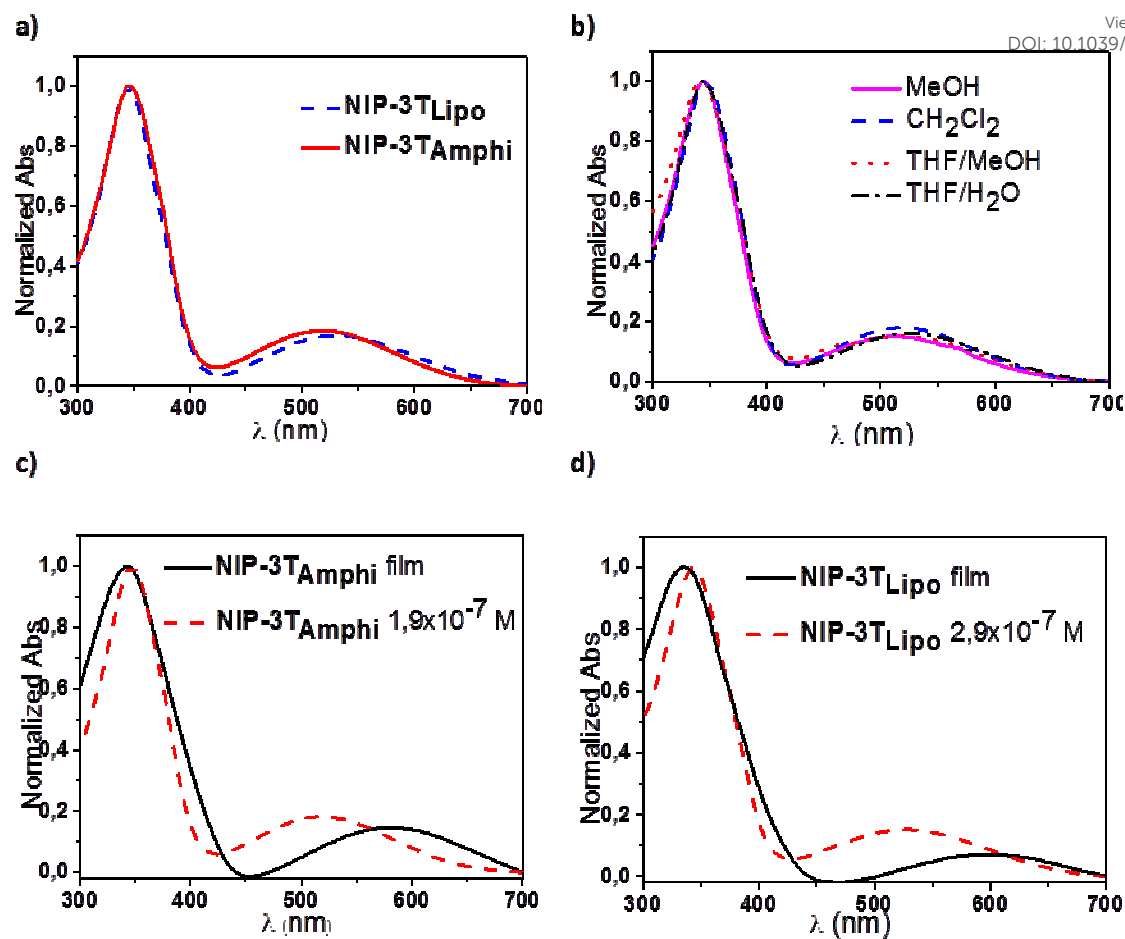
Figure 3. Normalized UV-vis spectra of (a) **NIP-3T$_{Lipo}$** (blue-dashed) and **NIP-3T$_{Amphi}$** (red-solid) (3.9×10^{-7} M) in dichloromethane; (b) **NIP-3T$_{Amphi}$** in different polar solvents; (c) **NIP-3T$_{Amphi}$** in dichloromethane solution (1.9×10^{-7} M, red dashed line) and in film (black solid line) and d) **NIP-3T$_{Lipo}$** in dichloromethane solution (2.9×10^{-7} M, blue solid line) and in film (red solid line).

These results prompt us to analyze molecular aggregation further. For this end, temperature dependent electronic absorption spectra were recorded in 2-methyltetrahydrofuran (Figure 4). In this case, significant changes were observed for the two semiconductors; while a severe bathochromic displacement (~50 nm) of the low energy band is observed for **NIP-3T$_{Amphi}$** upon cooling down, only negligible changes are recorded for **NIP-3T$_{Lipo}$**, indicating a stronger tendency to form aggregates for the amphiphilic molecule. **NIP-3T$_{Amphi}$** absorption spectrum at low temperature also shows a noticeable broadening of the high energy band, which is in agreement with the

formation of aggregates. On the contrary, the spectrum of **NIP-3T$_{Lipo}$** remains basically unaltered throughout the whole temperature range analyzed.
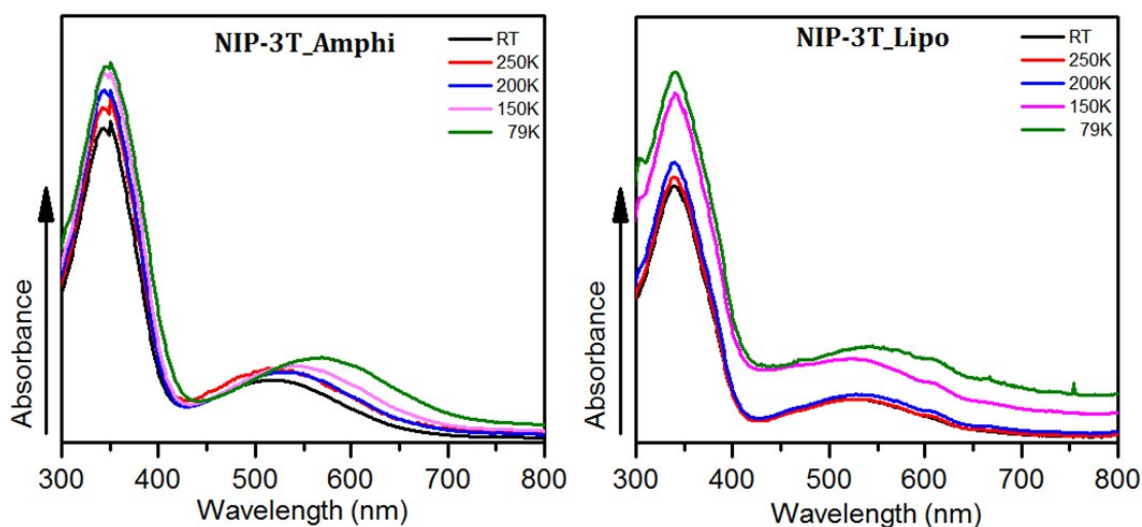
Figure 4. Temperature-dependent absorption spectra of **NIP-3T$_{Amphi}$** (left) and **NIP-3T$_{Lipo}$** (right).

Emission spectra at different temperatures (79K-305K) were also examined for the two derivatives (Figure 5). No spectral profile changes are found for **NIP-3T$_{Lipo}$** for the whole temperature range explored while the emission spectrum of **NIP-3T$_{Amphi}$** spectrum recorded at 79 K shows the appearance of a new emission band at approximately 485 nm, likely due to the stabilization of aggregates at low temperature.
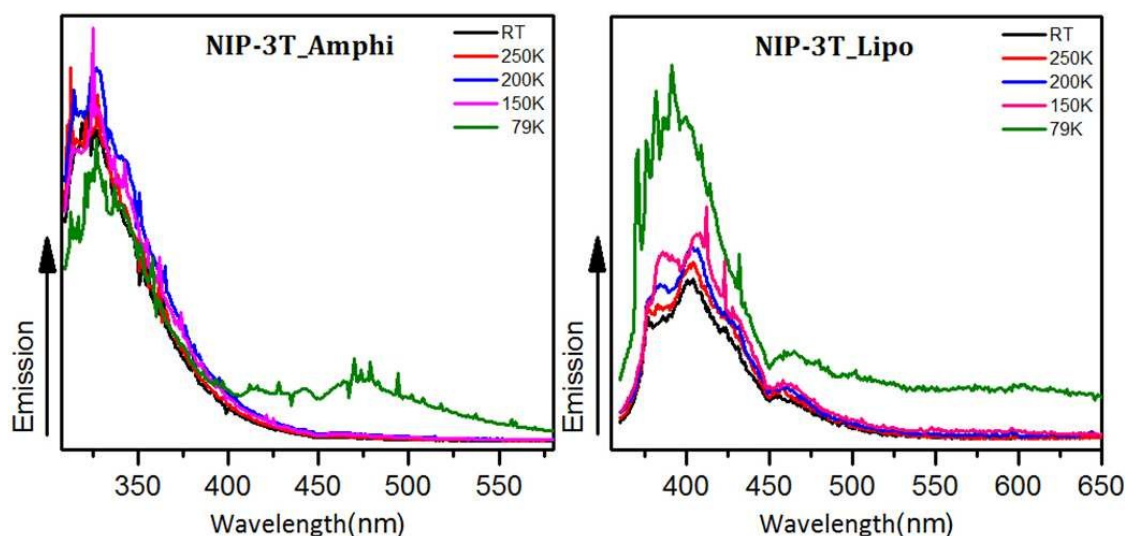

Figure 5.Temperature-dependent emission spectra.

The temperature dependence observed in the absorption and emission spectra of **NIP-3T_{Amphi}** is indicative of a stronger or at least a different tendency for aggregation of this amphiphilic derivative in comparison with the parent lipophilic analogue.

Unlike other previously reported amphiphilic oligothiophene-acceptor dyads,[24] newly designed dyads **NIP-3T_{Amphi}** and **NIP-3T_{Lipo}** in differential scanning calorimetry (DSC) did not show any LC mesophase. **NIP-3T_{Lipo}** exhibits just one phase transition during cooling, related to solidification from the isotropic melt at 67 °C while **NIP-3T_{Amphi}** did not show any phase transition (see Figures S8 and S9). The powder X-ray diffraction (XRD) analysis for **NIP-3T_{Lipo}** showed two peaks corresponding to d-spacings of 23.71 and 18.29 while **NIP-3T_{Amphi}** showed a set of four distinct peaks with d-spacings of 26.33, 16.88, 10.97 and 8.16 Å, thus reflecting the more ordered structure of the amphiphilic derivative (see Figures S10 and S11). Similar results are recorded for their corresponding thin films (Figure S12), showing **NIP-3T_{Amphi}** two peaks at 3.30 and 6.67 (second order reflection) and **NIP-3T_{Lipo}** one only peak at 3.97 degrees.

In order to assess the different tendency for aggregation in the two derivatives, a hexane solution (5mL) was heated at 60ºC until it turned clear. Then, the resulting solution was allowed to cool to 25 ºC, whereupon a suspension resulted for **NIP-3T_{Amphi}**. On the contrary, no aggregates were observed for **NIP-3T_{Lipo}** by this method. Scanning electron microscopy (SEM) of the suspension, after being air-dried, showed the presence of microfibers with a high aspect ratio and lengths surpassing 20 µm (Figure 6).
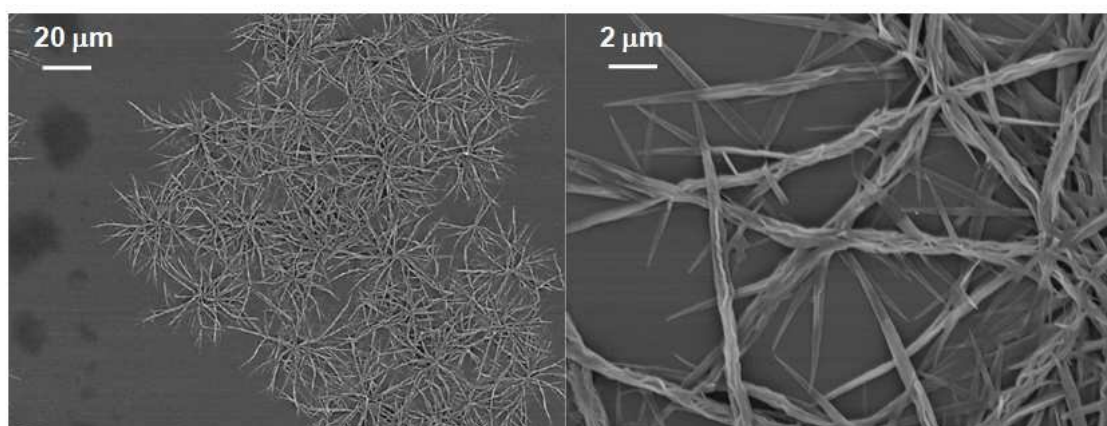

Figure 6. SEM micrographs of an air dried suspension of self-assembled **NIP-3T_{Amphi}**.

However, the growth of micrometer size rods of **NIP-3T$_{Lipo}$** was also feasible by using a good solvent/bad solvent solution mixture (CHCl$_3$/CH$_3$OH), as observed in the SEM images of Figure 7. Interestingly, **NIP-3T$_{Lipo}$** rods present a completely different morphology to those of **NIP-3T$_{Amphi}$**, pointing out to a different aggregation pattern. Rods lengths in this case are around 10 μm long. Although nanostructures growth for both compounds under similar conditions was not possible due to different solubility properties of the studied systems, from the SEM images it becomes clear that the resulting structures differ substantially upon introduction of polar alkyl chains.
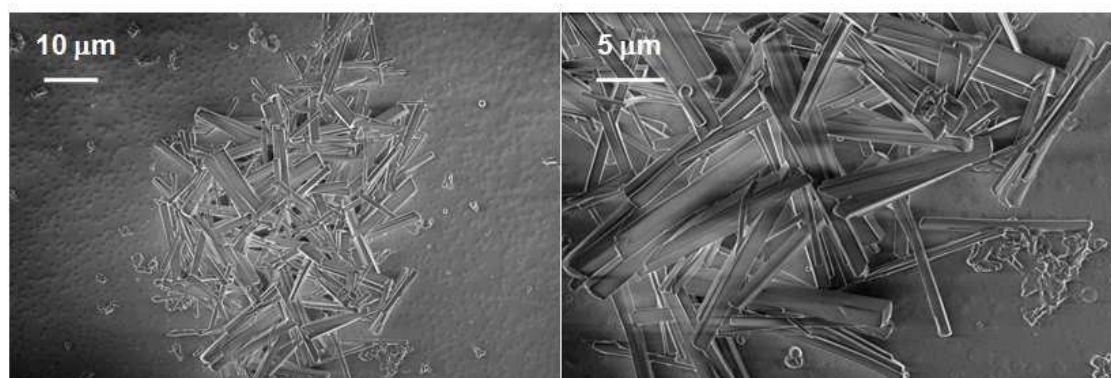

Figure 7. SEM micrographs of an air dried suspension of self-assembled **NIP-3T$_{Lipo}$**.

Since crystal growth of **NIP-3T$_{Amphi}$** and **NIP-3T$_{Lipo}$** was not possible, in order to elucidate the aggregation pattern, we carried out calculations of two different theoretical dimers for each molecule, one in a parallel (P) and the other in an antiparallel (AP) disposition (Figure 8). The estimation of the interaction energy of the aggregate was feasible at two different levels of calculations, CAM-B3LYP/6-31G** and M062X/6-31G** (Figure S13).[43-45]

The CAM-B3LYP[46] was chosen since it is a long-range corrected hybrid functional that allows better long-range connection effects on dimers than the widely used B3LYP functional.[47, 48] On the other hand, the M062X functional[49, 50] was used because of its ability to describe π-π interactions and estimate the energies of the weak intermolecular present in π-dimers.
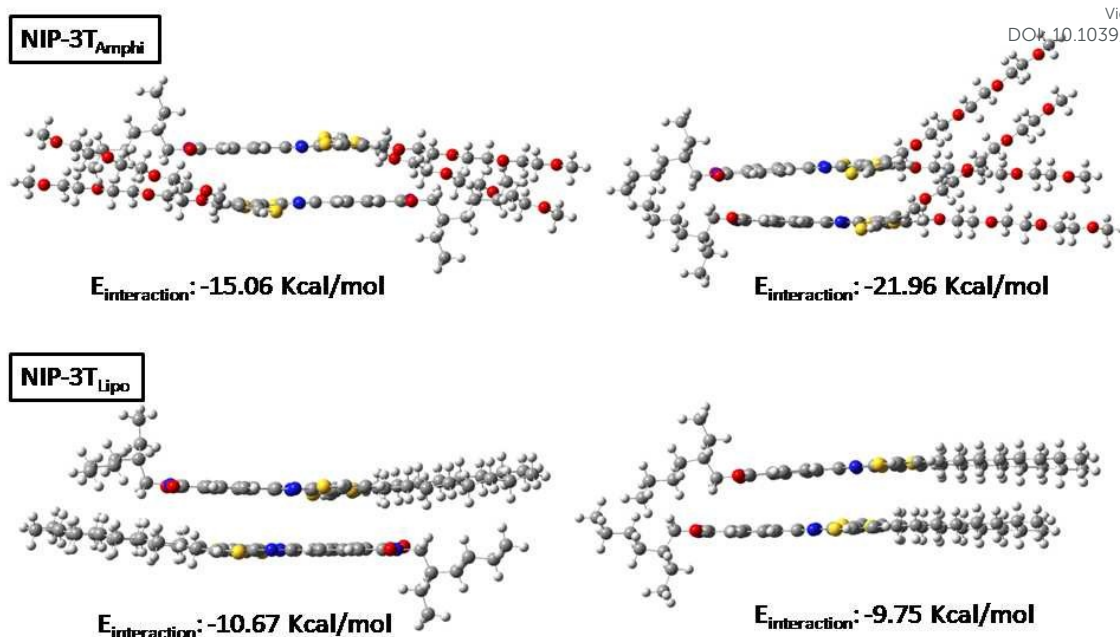
Figure 8. CAM-B3LYP/6-31G** estimated dimers (left: antiparallel configuration (AP) and right: parallel configuration (P)) for **NIP-3T$_{Amphi}$** and **NIP-3T$_{Lipo}$**.

Both levels of calculations predict that for the amphiphilic molecule, **NIP-3T$_{Amphi}$**, the most stable dimer is the parallel one (by 6.9 Kcal/mol at both the CAM-B3LYP and the M062X level), as expected, due to attractive interactions between the polar end groups. On the contrary, the antiparallel dimer model is slightly more stable (by ~1 Kcal/mol at the CAM-B3LYP level and 1.85 Kcal/mol at the M062X level) for the **NIP-3T$_{Lipo}$** system, as previously demonstrated for other oligothiophene-naphthalene fused molecules.[10] Since both approximations seem to be suitable to track this problem, for the remaining calculations we will make use of CAM-B3LYP functional.

Reorganization energies were calculated for the isolated molecules. A slightly increase of the energies for both electron and hole transfer was found for the amphiphilic derivative (λ_h: 264 meV, λ_e: 312 meV for **NIP-3T$_{Lipo}$** vs. λ_h: 281 meV, λ_e: 324 meV for **NIP-3T$_{Amphi}$**). Similar increases in reorganization energies upon alkoxy/alkylether substitution have been previously observed.[43, 51] Nevertheless, the values for both derivatives are within the common ones reported for active organic semiconductors. For instance, λ_h values of 306 meV and λ_e values of 309 meV were obtained for phenyl-substituted dithienoacene (DP-DTT) and phenyl-alkyl substituted perylene tetracarboxylic diimides for which hole and electron field-effect mobilities as high as 0.31 and 1.4 $cm^2V^{-1}s^{-1}$, respectively, were reported.[52, 53]

In addition, it is important to understand how the intermolecular packing influences fundamental charge-transport parameters, such as electronic coupling (or transfer integrals). To this end, transfer integrals (t) were calculated for the two predicted dimers (P and AP configurations) for each molecule (see Table 2). Larger t values for hole transport (t_h) are found in the P configuration when compared to those obtained in the AP configuration. This result is not surprising since the transfer integral is driven by wave function overlap, and a much lower HOMO-HOMO overlap occurs in the antiparallel disposition because the HOMO is basically located on the terthiophene fragment. However, since the LUMO is more delocalized over the conjugated framework molecule the t values for electrons (t_e) remains significant in the antiparallel disposition; note that even larger t_e values are found for **NIP-3T$_{Amphi}$(AP)** when compared to **NIP-3T$_{Amphi}$(P)**. The extremely low t_e values obtained for **NIP-3T$_{Amphi}$(P)** can be attributed to the displacement along the short molecular axis observed in this optimized dimer (see SI); note that these calculations are performed in the vacuum and some changes in the stacks are expected within the thin film. In order to give more insights in this respect, we have calculated the impact of short-axis displacement on the transfer integrals by sliding one molecule over the other in a cofacial configuration, without having to consider the substituents explicitly (see Figure S14). As a consequence of the larger present of nodal planes in the LUMO orbitals along the short molecular axes, the LUMO-LUMO overlap is much larger affected by small displacements between adjacent molecules in this direction when compared to the HOMO-HOMO overlap; therefore, short-axis displacement is expected to impact more strongly on the electron than hole transport.

Comparing the most stable dimeric configurations for each system (data highlighted in bold in Table 2), it is remarkably clear that while the transfer integral for electron transport remains basically unaltered with the amphiphilic (**NIP-3T$_{Amphi}$(P)**) /lipophilic (**NIP-3T$_{Lipo}$(AP)**) interactions, transfer integral for holes in **NIP-3T$_{Amphi}$(P)** is greatly enhanced, with a t_h value of 62 meV, which may be extremely interesting for hole transport.

Table 2. Calculated transfer integrals (in meV) for hole (t_h) and electron (t_e) transfer. AP denotes the theoretical dimer having an antiparallel disposition while P denotes the theoretical dimer having a parallel disposition. The most stable systems appear are highlighted in bold.

Molecule	t_h (meV)	t_e (meV)
NIP-3T$_{Amphi}$ (AP)	-34	36
NIP-3T$_{Amphi}$ (P)	**62**	**3**
NIP-3T$_{Lipo}$ (AP)	**-8**	**11**
NIP-3T$_{Lipo}$ (P)	23	-68

Therefore, despite the almost identical electronic parameters (HOMO, LUMO, bandgap) for both systems, their different aggregation behavior may play a role in their performance in optoelectronic devices. Thus, we found that the photoconducting properties, as well as the charge carrier mobility, of the amphiphilic derivative **NIP-3T$_{Amphi}$** are better than those of the parent lipophilic analogue.

In a first attempt, bottom-gate top contact field-effect transistors were fabricated. Semiconductors thin films were deposited either on untreated and SAM-treated Si/SiO$_2$. However, while untreated substrates give no field-effect performances, thin films on SAM-treated Si/SiO$_2$ was not possible for **NIP-3T$_{Amphi}$** due to the surface hydrophobicity, incompatible with its hydrophilic alkyl chains. Therefore, charge carriers mobility at RT was determined by employing the time of flight (TOF) technique.[54,55,56] Figure 9 shows, in a log-log scale, electron current transients in **NIP-3T$_{Amphi}$** and **NIP-3T$_{Lipo}$** samples, at room temperature (RT) under a field of 2 V/µm. Remarkably, the mobility at RT and 2 V/µm in **NIP-3T$_{Amphi}$** (4.3×10^{-6} cm^{-2} V^{-1} s^{-1}) is about 30 times higher than that in **NIP-3T$_{Lipo}$** (1.3×10^{-7} cm^{-2} V^{-1} s^{-1}). For both materials, the transients have similar behavior and can be qualitatively described with the stochastic theory of dispersive transport in amorphous solids of Scher and Moltroll (SM).[57] In this model, the transit time (τ), corresponding to the arrival of fastest carriers travelling a distance d, is determined from the maximum slope change in the final part of the curve. According to this, τ values have been obtained for **NIP-3T$_{Amphi}$** and **NIP-3T$_{Lipo}$**, respectively (see Figure 9). It is also observed that for times shorter than and longer than τ, the logarithmic slopes (m_1 and m_2, respectively) are higher and lower than -1 even though the sum is not -2, as predicted by the SM theory. This condition

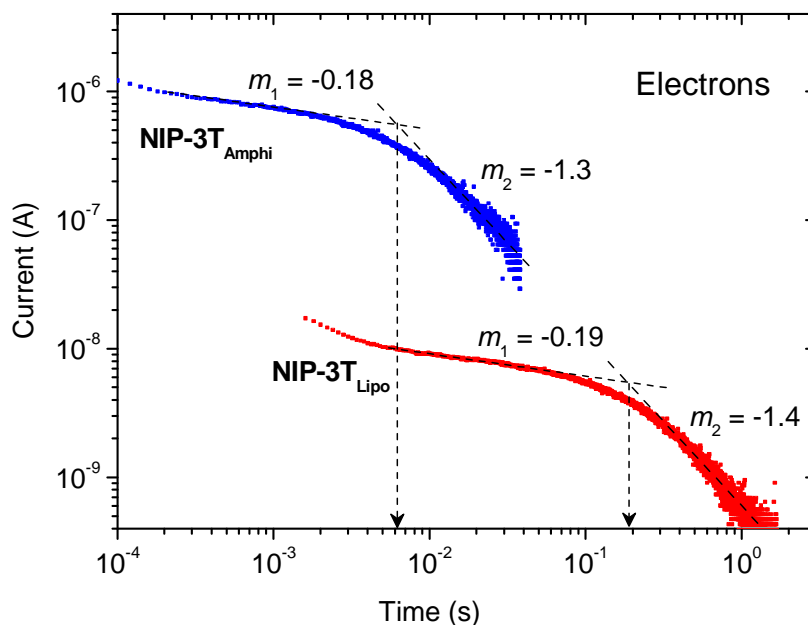however, is only an approximation and the sum is often found to be different than -2. [40] [42, 58] [59]

Figure 9. Electron current transients in **NIP-3T$_{Amphi}$** and **NIP-3T$_{Lipo}$** samples under a field of 2 V/µm. The slope values for times shorter and longer than the transit time τ, (m_1 and m_2, respectively) are shown in the plot.

Figure 10 shows in a log scale the RT mobility of electrons as a function of the square root of the applied field, $E^{1/2}$, for **NIP-3T$_{Amphi}$** and **NIP-3T$_{Lipo}$**. This representation is used because the mobility field-dependence in disorder molecular solids is expected to follow a Poole-Frenkel type behavior.[54] Both materials show a weak field-dependence, with a similar negative slope value. This tendency has been observed in different organic materials at low fields. [40-42,60,61]
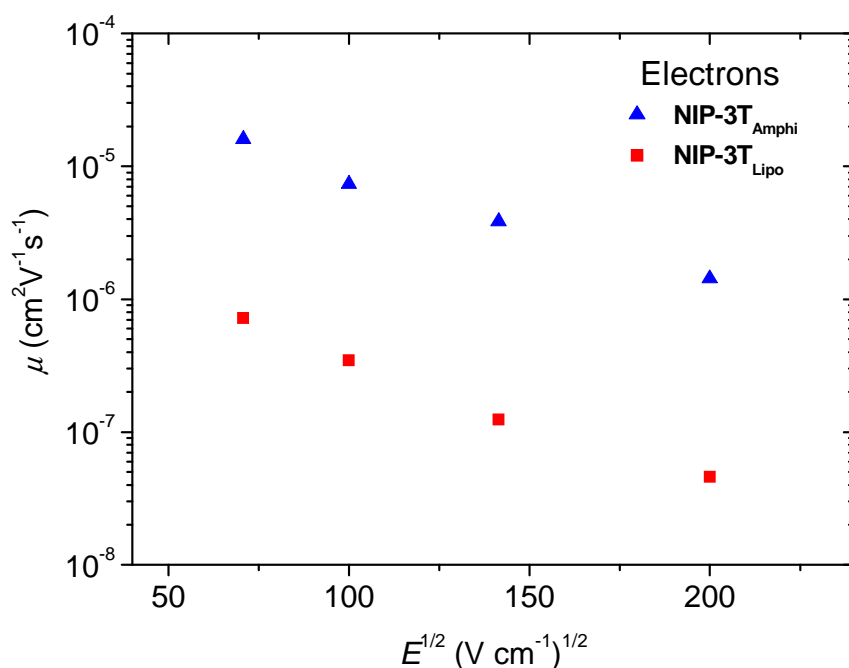
Figure 10. Poole-Frenkel plot of electron mobilities for **NIP-3T$_{Amphi}$** and **NIP-3T$_{Lipo}$** at RT.

Some additional experiments at RT and under a field of 2 V/µm were made to study hole transport. We found that the hole mobilities (2.1×10^{-6} cm^{-2} V^{-1} s^{-1} for **NIP-3T$_{Amphi}$** and 6.9×10^{-8} cm^{-2} V^{-1} s^{-1} for **NIP-3T$_{Lipo}$**) are approximately half of their corresponding electron mobilities, thus showing a relatively well balanced ambipolar transport. It should be noted that similarly to electron mobility, hole mobility is approximately 30 times higher in **NIP-3T$_{Amphi}$** than in **NIP-3T$_{Lipo}$**.

The photoconducting behavior of both materials has also been explored (see conditions in SI). This is a parameter of interest considering that photoconductive materials with low dimensionality have drawn intensive interest for their applications in photodetectors,[62-65] optical switches,[66,67-70] sensors[71-73] and photovoltaics.[15, 67, 74-76] It was found that photosensitivity is similar in both derivatives ($S \sim 10$). However, j_{phot} and j_{dark} are approximately 5 times higher for **NIP-3T$_{Amphi}$**. Besides, the photocurrent obtained under illumination through both, the positive and negative electrodes is quite similar, in agreement with the ambipolar behavior derived from mobility measurements.

The observation of a more efficient transport and photoconducting properties for the amphiphilic derivative can be attributed to the presence of suitably molecular stacking in molecular aggregates that reduce disorder and enhance transport.

Physical Chemistry Chemical Physics Accepted Manuscript

Physical Chemistry Chemical Physics Accepted Manuscript

Conclusions

We have developed amphiphilic and lipophilic donor-acceptor naphthalimide-oligothiophene assemblies which exhibit almost identical electronic parameters (HOMO, LUMO, bandgap) as determined from cyclic voltammetry and UV-Vis and fluorescence spectroscopies. In contrast with the similar molecular properties, both systems differ in their tendency for aggregation. While well-defined microfibers with lengths clearly surpassing 20 μm are easily grown for the **NIP-3T$_{Amphi}$** derivative, **NIP-3T$_{Lipo}$** grown rods are around 10 μm long. Interestingly, the morphologies of both aggregates differ substantially, pointing out a different aggregation pattern probably induced by amphiphilic and lipophilic interactions. Thus, aided by DFT molecular calculations, it was demonstrated that while the most stable configuration for a dimer stack of the lipophilic derivative shows an antiparallel disposition, the amphiphilic molecular design fosters the stabilization of a face to face parallel molecular stacking that reduce disorder and enhance the charge transport ability and photoconducting properties of this type of materials.

Acknowledgements

References

1. M.-H. Yoon, S. A. DiBenedetto, A. Facchetti and T. J. Marks, *Journal of the American Chemical Society*, 2005, **127**, 1348-1349.
2. S. Ando, J.-i. Nishida, H. Tada, Y. Inoue, S. Tokito and Y. Yamashita, *Journal of the American Chemical Society*, 2005, **127**, 5336-5337.
3. N. Sakai, J. Mareda, E. Vauthey and S. Matile, *Chemical Communications*, 2010, **46**, 4225-4237.
4. R. M. Duke, E. B. Veale, F. M. Pfeffer, P. E. Kruger and T. Gunnlaugsson, *Chemical Society Reviews*, 2010, **39**, 3936-3953.
5. H. E. Katz, A. J. Lovinger, J. Johnson, C. Kloc, T. Siegrist, W. Li, Y. Y. Lin and A. Dodabalapur, *Nature*, 2000, **404**, 478-481.

6.   W. Huang, J. Sinha, M.-L. Yeh, J. F. M. Hardigree, R. LeCover, K. Besar, A. M. Rule, P. N. Breysse and H. E. Katz, *Advanced Functional Materials*, 2013, **23**, 4094-4104.

7.   T. Weil, T. Vosch, J. Hofkens, K. Peneva and K. Müllen, *Angewandte Chemie International Edition*, 2010, **49**, 9068-9093.

8.   F. Wurthner and M. Stolte, *Chemical Communications*, 2011, **47**, 5109-5115.

9.   J. L. Segura, H. Herrera and P. Bauerle, *Journal of Materials Chemistry*, 2012, **22**, 8717-8733.

10.   R. P. Ortiz, H. Herrera, R. Blanco, H. Huang, A. Facchetti, T. J. Marks, Y. Zheng and J. L. Segura, *Journal of the American Chemical Society*, 2010 **132**, 8440-8452.

11.   R. P. Ortiz, H. Herrera, C. Seoane, J. L. Segura, A. Facchetti and T. J. Marks, *Chemistry – A European Journal*, 2012, **18**, 532-543.

12.   R. Ponce Ortiz , H. Herrera, M. J. Mancheño, C. Seoane, J. L. Segura, P. Mayorga Burrezo, J. Casado, J. T. López Navarrete, A. Facchetti and T. J. Marks, *Chemistry – A European Journal*, 2013, **19**, 12458-12467.

13.   V. Percec, M. Glodde, T. K. Bera, Y. Miura, I. Shiyanovskaya, K. D. Singer, V. S. K. Balagurusamy, P. A. Heiney, I. Schnell, A. Rapp, H. W. Spiess, S. D. Hudson and H. Duan, *Nature*, 2002, **417**, 384-387.

14.   W. Pisula, M. Kastler, D. Wasserfallen, J. W. F. Robertson, F. Nolde, C. Kohl and K. Müllen, *Angewandte Chemie International Edition*, 2006, **45**, 819-823.

15.   P. Jonkheijm, N. Stutzmann, Z. Chen, D. M. de Leeuw, E. W. Meijer, A. P. H. J. Schenning and F. Würthner, *Journal of the American Chemical Society*, 2006, **128**, 9535-9540.

16.   A. de la Peña, I. Arrechea-Marcos, M. J. Mancheño, M. C. Ruiz Delgado, J. T. López Navarrete, J. L. Segura and R. Ponce Ortiz, *Chemistry – A European Journal*, 2016, **22**, 13643-13652.

17.   S. Günes, H. Neugebauer and N. S. Sariciftci, *Chemical Reviews*, 2007, **107**, 1324-1338.

18.   G. Dennler, M. C. Scharber and C. J. Brabec, *Advanced Materials*, 2009, **21**, 1323-1338.

19.   J. Roncali, *Accounts of Chemical Research*, 2009, **42**, 1719-1730.

20.   Y.-J. Cheng, S.-H. Yang and C.-S. Hsu, *Chemical Reviews*, 2009, **109**, 5868-5923.

21.   L. Dou, J. You, Z. Hong, Z. Xu, G. Li, R. A. Street and Y. Yang, *Advanced Materials*, 2013, **25**, 6642-6671.

22.   A. J. Heeger, *Advanced Materials*, 2014, **26**, 10-28.

23.   J. W. Rumer and I. McCulloch, *Materials Today*, 2015, **18**, 425-435.

24.   W.-S. Li, Y. Yamamoto, T. Fukushima, A. Saeki, S. Seki, S. Tagawa, H. Masunaga, S. Sasaki, M. Takata and T. Aida, *Journal of the American Chemical Society*, 2008, **130**, 8886-8887.

25.   W.-S. Li, A. Saeki, Y. Yamamoto, T. Fukushima, S. Seki, N. Ishii, K. Kato, M. Takata and T. Aida, *Chemistry – An Asian Journal*, 2010, **5**, 1566-1572.

26.   S. Prasanthkumar, S. Ghosh, V. C. Nair, A. Saeki, S. Seki and A. Ajayaghosh, *Angewandte Chemie International Edition*, 2015, **54**, 946-950.

27.   *Annual Review of Materials Research*, 2016, **46**, 235-262.

28.   S. Ghosh, D. S. Philips, A. Saeki and A. Ajayaghosh, *Advanced Materials*, 2016, n/a-n/a.

29.   S. Prasanthkumar, A. Saeki, S. Seki and A. Ajayaghosh, *Journal of the American Chemical Society*, 2010, **132**, 8866-8867.

30.   S. Prasanthkumar, A. Gopal and A. Ajayaghosh, *Journal of the American Chemical Society*, 2010, **132**, 13206-13207.

31.   K. Sakakibara, P. Chithra, B. Das, T. Mori, M. Akada, J. Labuta, T. Tsuruoka, S. Maji, S. Furumi, L. K. Shrestha, J. P. Hill, S. Acharya, K. Ariga and A. Ajayaghosh, *Journal of the American Chemical Society*, 2014, **136**, 8548-8551.

32.   S. S. Babu, V. K. Praveen and A. Ajayaghosh, *Chemical Reviews*, 2014, **114**, 1973-2129.

33.   L. Wang, H. Liu and J. Hao, *Chemical Communications*, 2009, 1353-1355.

34.   W. Cai, G.-T. Wang, Y.-X. Xu, X.-K. Jiang and Z.-T. Li, *Journal of the American Chemical Society*, 2008, **130**, 6936-6937.

35.   H. Shao, J. Seifert, N. C. Romano, M. Gao, J. J. Helmus, C. P. Jaroniec, D. A. Modarelli and J. R. Parquette, *Angewandte Chemie International Edition*, 2010, **49**, 7688-7691.

36.   S. V. Bhosale, C. H. Jani, C. H. Lalander, S. J. Langford, I. Nerush, J. G. Shapter, D. Villamaina and E. Vauthey, *Chemical Communications*, 2011, **47**, 8226-8228.

37.   S. Ghosh, X.-Q. Li, V. Stepanenko and F. Würthner, *Chemistry – A European Journal*, 2008, **14**, 11343-11357.

38.   H. Herrera, P. de Echegaray, M. Urdanpilleta, M. J. Mancheno, E. Mena-Osteritz, P. Bauerle and J. L. Segura, *Chemical Communications*, 2013, **49**, 713-715.

39.   C. Kitamura, S. Tanaka and Y. Yamashita, *Chemistry of Materials*, 1996, **8**, 570-578.

40.   R. P. Ortiz, J. Casado, V. Hernández, J. T. L. Navarrete, J. A. Letizia, M. A. Ratner, A. Facchetti and T. J. Marks, *Chemistry – A European Journal*, 2009, **15**, 5023-5039.

41.   M. Dal Colle, C. Cova, G. Distefano, D. Jones, A. Modelli and N. Comisso, *The Journal of Physical Chemistry A*, 1999, **103**, 2828-2835.

42.   M.-H. Yoon, S. A. DiBenedetto, M. T. Russell, A. Facchetti and T. J. Marks, *Chemistry of Materials*, 2007, **19**, 4864-4881.

43.   M. C. R. Delgado, E.-G. Kim, D. A. d. S. Filho and J.-L. Bredas, *Journal of the American Chemical Society*, 2010, **132**, 3375-3387.

44.   T. Mori, Y. Inoue and S. Grimme, *The Journal of Organic Chemistry*, 2006, **71**, 9797-9806.

45.   G. García, M. Moral, J. M. Granadino-Roldán, A. Garzón, A. Navarro and M. Fernández-Gómez, *The Journal of Physical Chemistry C*, 2013, **117**, 15-22.

46.   T. Yanai, D. P. Tew and N. C. Handy, *Chemical Physics Letters*, 2004, **393**, 51-57.

47.   W. J. Hehre, R. Ditchfield and J. A. Pople, *The Journal of Chemical Physics*, 1972, **56**, 2257-2261.

48.   M. M. Francl, W. J. Pietro, W. J. Hehre, J. S. Binkley, M. S. Gordon, D. J. DeFrees and J. A. Pople, *The Journal of Chemical Physics*, 1982, **77**, 3654-3665.

49.   Y. Zhao and D. G. Truhlar, *Accounts of Chemical Research*, 2008, **41**, 157-167.

50.   K. E. Riley, M. Pitoňák, J. Černý and P. Hobza, *Journal of Chemical Theory and Computation*, 2010, **6**, 66-80.

51.   S. Salman, M. C. R. Delgado, V. Coropceanu and J.-L. Brédas, *Chemistry of Materials*, 2009, **21**, 3593-3601.

52. Y. M. Sun, Y. Q. Ma, Y. Q. Liu, Y. Y. Lin, Z. Y. Wang, Y. Wang, C. A. Di, K. Xiao, X. M. Chen, W. F. Qiu, B. Zhang, G. Yu, W. P. Hu and D. B. Zhu, *Advanced Functional Materials*, 2006, **16**, 426-432.

53. J. H. Oh, H. W. Lee, S. Mannsfeld, R. M. Stoltenberg, E. Jung, Y. W. Jin, J. M. Kim, J.-B. Yoo and Z. Bao, *Proceedings of the National Academy of Sciences*, 2009, **106**, 6065-6070.

54. J. A. Quintana, J. M. Villalvilla, A. de la Peña, J. L. Segura and M. A. Díaz-García, *The Journal of Physical Chemistry C*, 2014, **118**, 26577-26583.

55. Y. Shirota and H. Kageyama, *Chemical Reviews*, 2007, **107**, 953-1010.

56. K.Wong, Ohio State University, 2003.

57. H. Scher and E. W. Montroll, *Physical Review B*, 1975, **12**, 2455-2477.

58. H. Bässler, *physica status solidi (b)*, 1993, **175**, 15-56.

59. S. A. Choulis, Y. Kim, J. Nelson, D. D. C. Bradley, M. Giles, M. Shkunov and I. McCulloch, *Applied Physics Letters*, 2004, **85**, 3890-3892.

60. G. Juška, K. Genevičius, K. Arlauskas, R. Österbacka and H. Stubb, *Physical Review B*, 2002, **65**, 233208.

61. S. Raj Mohan, M. P. Joshi and M. P. Singh, *Chemical Physics Letters*, 2009, **470**, 279-284.

62. Y. Ahn, J. Dunning and J. Park, *Nano Letters*, 2005, **5**, 1367-1370.

63. J. Wang, M. S. Gudiksen, X. Duan, Y. Cui and C. M. Lieber, *Science*, 2001, **293**, 1455-1457.

64. H. Kind, H. Yan, B. Messer, M. Law and P. Yang, *Advanced Materials*, 2002, **14**, 158-160.

65. G. A. O'Brien, A. J. Quinn, D. A. Tanner and G. Redmond, *Advanced Materials*, 2006, **18**, 2379-2383.

66. Y. Xia, P. Yang, Y. Sun, Y. Wu, B. Mayers, B. Gates, Y. Yin, F. Kim and H. Yan, *Advanced Materials*, 2003, **15**, 353-389.

67. Y. Yamamoto, T. Fukushima, Y. Suna, N. Ishii, A. Saeki, S. Seki, S. Tagawa, M. Taniguchi, T. Kawai and T. Aida, *Science*, 2006, **314**, 1761-1764.

68. A. D. Schwab, D. E. Smith, B. Bond-Watts, D. E. Johnston, J. Hone, A. T. Johnson, J. C. de Paula and W. F. Smith, *Nano Letters*, 2004, **4**, 1261-1265.

69. L. Jiang, Y. Fu, H. Li and W. Hu, *Journal of the American Chemical Society*, 2008, **130**, 3937-3941.

70. Y. Zhang, P. Chen, L. Jiang, W. Hu and M. Liu, *Journal of the American Chemical Society*, 2009, **131**, 2756-2757.

71. J. Gong, Y. Li, X. Chai, Z. Hu and Y. Deng, *The Journal of Physical Chemistry C*, 2010, **114**, 1293-1298.

72. C. Lao, Y. Li, C. P. Wong and Z. L. Wang, *Nano Letters*, 2007, **7**, 1323-1328.

73. D. Wang, C. Hao, W. Zheng, Q. Peng, T. Wang, Z. Liao, D. Yu and Y. Li, *Advanced Materials*, 2008, **20**, 2628-2632.

74. F. Würthner, Z. Chen, F. J. M. Hoeben, P. Osswald, C.-C. You, P. Jonkheijm, J. v. Herrikhuyzen, A. P. H. J. Schenning, P. P. A. M. van der Schoot, E. W. Meijer, E. H. A. Beckers, S. C. J. Meskers and R. A. J. Janssen, *Journal of the American Chemical Society*, 2004, **126**, 10611-10618.

75. A. L. Sisson, N. Sakai, N. Banerji, A. Fürstenberg, E. Vauthey and S. Matile, *Angewandte Chemie International Edition*, 2008, **47**, 3727-3729.

76. Y. Yamamoto, G. Zhang, W. Jin, T. Fukushima, N. Ishii, A. Saeki, S. Seki, S. Tagawa, T. Minari, K. Tsukagoshi and T. Aida, *Proceedings of the National Academy of Sciences*, 2009, **106**, 21051-21056.